Bacterial Swarming: A Biochemical Time-Resolved FTIR−ATR Study of *Proteus mirabilis* Swarm-Cell Differentiation

Michaël Gué, Virginie Dupont, Alain Dufour, and Olivier Sire*

Laboratoire de Biologie et Chimie Moléculaires, Université de Bretagne Sud, Campus de Tohannic, B.P. 573, 56017 Vannes Cedex, France

Received March 5, 2001; Revised Manuscript Received July 23, 2001

ABSTRACT: Fourier transform infrared spectroscopy was applied to the study of the differentiation process undergone by *Proteus mirabilis*. This bacterium exhibits a remarkable dimorphism, allowing the cells to migrate on a solid substratum in a concerted manner yielding characteristic ring patterns. We performed an in situ noninvasive analysis of biochemical events occurring as vegetative cells differentiate into elongated, multinucleate, nonseptate, and hyperflagellated swarm cells. The major findings arising from this study are (i) the real-time monitoring of flagellar filament assembly, (ii) the evidence for de novo synthesis of qualitatively different lipopolysaccharides (LPS) and/or exopolysaccharides (EPS) constituting the slime into which bacteria swarm, and (iii) the alteration in the membrane fatty acid composition with a concomitant 10 °C decrease in the gel/liquid crystal phase transition resulting in an elevated membrane fluidity in swarm cells at the growth temperature. The time course of events shows that the EPS−LPS syntheses are synchronous with membrane fatty acid alterations and occur about 1 h before massive flagellar filament assembly is detected. This study not only provided a time sketch of biochemical events involved in the differentiation process but also led to the identification of the major spectral markers of both vegetative and swarm cells. This identification will allow to resolve the time−space structure of *P. mirabilis* colonies by using infrared microscopy.

Every living process is embedded in a unique temporal grid. Disregarding the entity considered, molecule, cell, or organism, its characteristic properties rely on elementary phenomena exhibiting particular frequencies: protein fluctuations, oscillating enzymatic reactions, cellular divisions, etc. This temporal axis is too often disregarded in our attempts to describe the mechanisms of life. A bacterial colony behaves as an entity in which biochemical modifications occur in a concerted manner. Hence, the growth and behavior of individual cells become correlated in time and space to those of the whole population, which can be considered as a multicellular organism (*1*, *2*). Bacterial colonies are experimental systems of choice for studying fundamental problems of self-organization and pattern formation by complex biological systems. Such coordinated multicellular behaviors are particularly well exemplified by bacterial swarming, which is a form of active surface motility widespread among flagellated, Gram-negative bacteria (*3*−*5*). We used the uropathogenic *Proteus mirabilis* as a model since it is one of the bacteria exhibiting the strongest swarming abilities. From a central inoculum, a *P. mirabilis* colony is able to spread over the entire surface of a Petri plate within a few hours, by alternating periods of active mass migration and of cell division without colony expansion (consolidation) (*5*−*8*). As a result of this periodicity and of the cell coordination, the final colony displays a concentric ring pattern. The colony is encapsulated into an extracellular slime, which is a complex mixture including polysaccharides, surfactants, proteins, peptides, etc. The slime acts as a surface lubricant, provides an aqueous environment allowing flagella rotation, and is likely involved in cell−cell communications (*9*). Three *Proteus* capsular polysaccharides (CPS)[1] have been described (*10*), including a colony migration factor (Cmf), which is part of the slime and has been shown to facilitate *P. mirabilis* mass migration (*11*). This striking swarming behavior has driven microbiologists to study the genetic bases of the morphogenesis during which short (2 μm) vegetative swimming bacteria differentiate into elongated (40 μm or more), multinucleate, nonseptate, and hyperflagellated swarm cells (*6*, *12*, *13*). As the differentiated cells display enhanced properties of invasion of human urothelial cells and of production of a number of virulence factors (*14*−*17*), it is likely that the swarming behavior does not constitute a laboratory artifact but is essential to *P. mirabilis* pathogenicity and warrants for its ability to colonize urinary tracts (*17*) or to block catheters with crystalline biofilms (*18*). To undertake their differentiation, the bacteria must meet a number of requirements, such as the contact with a solid substratum, the presence of glutamine (*19*), the ability to assemble flagella (*20*, *21*), or a sufficient cell density (*22*).

* Corresponding author: e-mail, osire@univ-ubs.fr; tel, 33 297 683 172; fax, 33 297 681 639.

[1] Abbreviations: ATR, attenuated total reflection; Cmf, colony migration factor; CPS, capsular polysaccharide; DAPI, 4,6-diamidino-2-phenylindole; EPS, exopolysaccharides; FTIR, Fourier transform infrared; GC, gas chromatography; IR, infrared; LB, Luria−Bertani culture medium; LPS, lipopolysaccharides; PBS, phosphate-buffered saline (pH 7.2) (137 mM NaCl, 2.7 mM KCl, 1.5 mM KH_2PO_4, 8.1 mM Na_2HPO_4); PMSF, phenylmethanesulfonyl fluoride; SDS−PAGE, sodium dodecyl sulfate−polyacrylamide gel electrophoresis; TCA, trichloroacetic acid; TEN, Tris−EDTA−NaCl buffer [10 mM Tris-HCl (pH 8.0), 1 mM EDTA, 100 mM NaCl].

10.1021/bi010434m CCC: $20.00
Published on Web 09/06/2001

The genetic studies were successful in identifying key events leading to the differentiation (*5*), such as the regulation of the master operon *flhDC* and of its products (*23*−*27*), which induce flagellar gene expression and affect cell division (*28*−*30*). However, genetics did not reveal the dynamics of interactions involved in the long-range correlations which occur during swarming. As a matter of example, it cannot explain why a differentiated bacterium loses its mobility if isolated from the parent colony (*16*). This implies that swarming must somehow link all of the cells along the surface into one network of communication. The dynamics of formation of such symmetrical patterns must rely on a high-order information processing or on a global regulatory network. This, in turn, must imply that cells continuously exchange signals (multiple feedback within a population of more than 10^6 individuals) which can be of chemical or physicochemical nature. Such signals could be extracellular peptides and/or amino acids (*5*) but could also include membrane alterations (*3*). Hence, bacterial populations can generate dynamic, collective, "multicellular" actions through interplay of biological and physical factors that operate at a macroscopic level (*1*, *2*).

As mentioned above, although a number of studies have been performed to reveal the genetic regulation of *P. mirabilis* morphogenesis, few attempts have been made to investigate the underlying biochemical events. This maybe partly arises from limitations in our ability to devise conceptual and methodological approaches to address the problem. Here we present an experimental approach, which opens up the possibility of resolving, both spatially and temporally, the structure of a *P. mirabilis* colony by infrared microscopy. Fourier transform infrared spectroscopy in the attenuated total reflection mode (FTIR−ATR) is well suited to study biomaterial surfaces and biochemical events at biomaterial surfaces. However, the accurate time and space mapping of a colony requires the identification of spectral markers of both vegetative (nondifferentiated) and swarm cells, as well as a knowledge of the time course of the differentiation process. The present study focuses on events occurring during differentiation in slime, at the cell surface and in the membranes, for two reasons. First, it is largely admitted that the bacterial envelopes constitute major sensors of the environment and hence should respond and adapt to environmental changes. Second, membrane and cell surface molecular constituents significantly show up in IR spectra of living cells. In addition to biochemical studies, the thermotropic response of the membrane fatty acid ν_{CH_2} stretching frequency was investigated to probe the membrane gel/liquid crystal phase transition in both vegetative and swarm cells.

MATERIALS AND METHODS

Strain, Media, and Culture Conditions. The *P. mirabilis* wild-type strain WT19 corresponds to the clinical isolate U6450 (*6*). WT19 was grown in LB medium at 37 °C. To obtain homogeneous populations of differentiating bacteria, 200 μL of an overnight liquid culture was spread onto a LB agar (1.5%) plate, and the latter was incubated for various periods (from 0 to 6 h) at 37 °C (*20*).

Examination of the Level of Bacterial Elongation and of Population Homogeneity. The cells were resuspended in LB with 1% formaldehyde, and 4′,6-diamino-2-phenylindole (DAPI) was added to a final concentration of 0.25 $\mu g \cdot mL^{-1}$. DAPI is a fluorescent dye allowing the visualization of bacterial chromosomes (*31*), which was achieved by examination under an epifluorescence microscope (Olympus BX-60) with UV excitation and visible emission (380 nm cutoff). The elongation level was assessed by counting the number of nucleoids per cell as well as by measuring the bacterial rod lengths.

Flagellar Filament Extraction. The extracellular parts of flagella, the filaments, were broken by vortexing for 10 min bacteria resuspended in PBS and diluted to obtain an OD_{600} of 0.5. After centrifugation at 12000*g* for 5 min, the filament-containing supernatants were recovered. For subsequent infrared analyses, the filaments were concentrated using a microcon centrifugal filter device (microcon-100, Millipore). Filaments were checked for purity by SDS−PAGE. Accordingly, proteins from the supernatants were precipitated with 10% trichloroacetic acid and resuspended in a 1:1 mix of 0.1 N NaOH−SDS−PAGE sample buffer. The proteins were separated on a 12% polyacrylamide gel and stained with Coomassie brilliant blue.

Membrane Purification. Membrane extractions from *P. mirabilis* were based on a method described for *Lactococcus lactis* cells (*32*). Cells were harvested from a 50 mL culture by centrifugation (4000*g*, 10 min, 4 °C) and washed with 6.2 mL of TEN buffer, and the suspension was again centrifuged at 4000*g* for 10 min at 4 °C. The pellet resuspended in 400 μL of TEN buffer was diluted with 400 μL of the same buffer containing 12.5 $\mu g \cdot mL^{-1}$ lysozyme. After incubation at room temperature for 30 min, PMSF, $MgCl_2$, and NaCl were added to obtain final concentrations of 2, 10, and 500 mM, respectively. The suspension was diluted with 1 volume (1 mL) of 10 mM Tris-HCl buffer (pH 8.0) containing 20 and 30 $\mu g \cdot mL^{-1}$ DNase and RNase, respectively, and incubated on ice for 20 min. After centrifugation (2000*g*, 15 min, 4 °C), the supernatant was carefully removed, and the pellet was resuspended in 15 mL of 10 mM Tris-HCl (pH 8.0). The sedimentation of membrane vesicles was achieved by an additional centrifugation at 100000*g* and 4 °C for 60 min. Finally, the pellet was suspended in 400 μL of 50 mM Tris-HCl (pH 8.0) containing 10 mM $MgSO_4$ and stored at −20 °C.

Polysaccharide Purification. Differentiated cells and their exo products were removed from the agar by gentle washing to prevent cell lysis with ice-cold PBS supplemented with 0.15 mM $CaCl_2$ and 0.5 mM $MgCl_2$ and centrifuged (4000*g*, 10 min, 4 °C). The pellet containing the cells was washed with 25 mL of ice-cold PBS and centrifuged three times for further LPS extraction, whereas the supernatant (about 20 mL) was diluted to 50 mL with distilled water for EPS extraction. LPS and EPS fractions were purified by phenol/water extraction as previously described (*33*). The last pellet containing the LPS or EPS fraction was resuspended in pure water and stored at −20 °C until IR spectra acquisition.

Fatty Acid Analysis. The phospholipids were extracted from purified membranes fractions by the method of Folch et al. (*34*). The solvents were eliminated under vacuum, and the phospholipids were stored in a mixture of $C_2H_5OH-C_2H_5OC_2H_5$ (3:1). To obtain the fatty acid methyl esters, phospholipids were methanolyzed (0.5 $mol \cdot L^{-1}$ methanolic KOH, 5 min, 60 °C), and the methylation was performed in

the presence of BF_3-Et_2O. The resulting methyl esters were extracted with hexane.

Gas Chromatography. The GC experiments were performed with a Hewlett-Packard HP 6890 gas chromatograph equipped with a flame ionization detector. The 25 m long capillary column was filled with CP WAX 58 (Chrompack), and the carrier gas was helium. The fatty methyl esters were analyzed with a temperature gradient (100 °C for 1 min, rise 5°/min up to 200 °C, 200 °C for 1 min, rise 1 °C/min up to 240 °C, and then 240 °C for 10 min) and identified by comparing the retention times to those of a mixture of standard methyl esters (Supelco, fatty methyl ester mixture 47885-U).

Infrared Experiments. FTIR spectra were collected at 37 °C on a Portégé spectrometer (Nicolet) equipped with a thermostated horizontal ATR device (Specac) and a deuterated triglycine sulfate (DTGS) detector and obtained by coaddition of 256 interferograms. Resolution was set to 2 cm^{-1}. The interferograms were apodized with a Happ−Genzel function and Fourier transformed with one level of zero filling to yield data encoded every 0.48 cm^{-1}. All spectra were analyzed with software written at the National Research Council of Canada (*35*). Time analysis of the differentiation process was achieved by coating a 60° germanium horizontal ATR crystal with an upside-down strip of agar freshly cut out of a Petri dish to fit the size of the crystal. Agar strips and the corresponding spectra were collected every 15 min for 6 h from a set of about 10 Petri dishes. Three independent experiments have been performed.

FTIR spectra of purified membrane fractions were recorded from 2 to 60 °C at 1 °C intervals. To reduce water-induced distortions, the membrane pellets were prepared as gel films between AgBr windows (50 μm path length) and sealed in the IR cuvette. The cuvette was placed in a variable temperature cell (Graseby Specac) cooled by a liquid nitrogen dewar. Temperature was monitored by an automatic temperature controller (Specac), the thermocouple being located inside the steel jacket surrounding the cell. The temperature controller was set to 2 °C for 15 min to allow the sample to equilibrate; then the temperature was linearly increased at a 0.5 °C min^{-1} rate up to 60 °C while one averaged FTIR spectrum was effectively collected and stored per 1 °C.

To enhance the level of confidence in the determination of the frequencies of bands of interest, raw spectra were split in subspectra and further analyzed by inspecting their inverted second derivative spectra (*36*) with an optimal break point of 0.2 (*35*).

RESULTS

Time Course of Biochemical Events Associated to P. mirabilis Differentiation. FTIR−ATR spectra of homogeneous populations of vegetative or differentiating *P. mirabilis* were collected every 15 min for 6 h to resolve the time course of biochemical events linked to the differentiation process. As seen from Figure 1, the differentiation was checked by visually monitoring the elongation state with DAPI-labeled bacteria, which allows counting the number of nucleoids per cell. This indicates the elongation level, since differentiated bacteria contain one nucleoid per unit length (*16*). In our experimental conditions, the elongation process was initiated about 60 min after plating and was achieved within 5 h, since

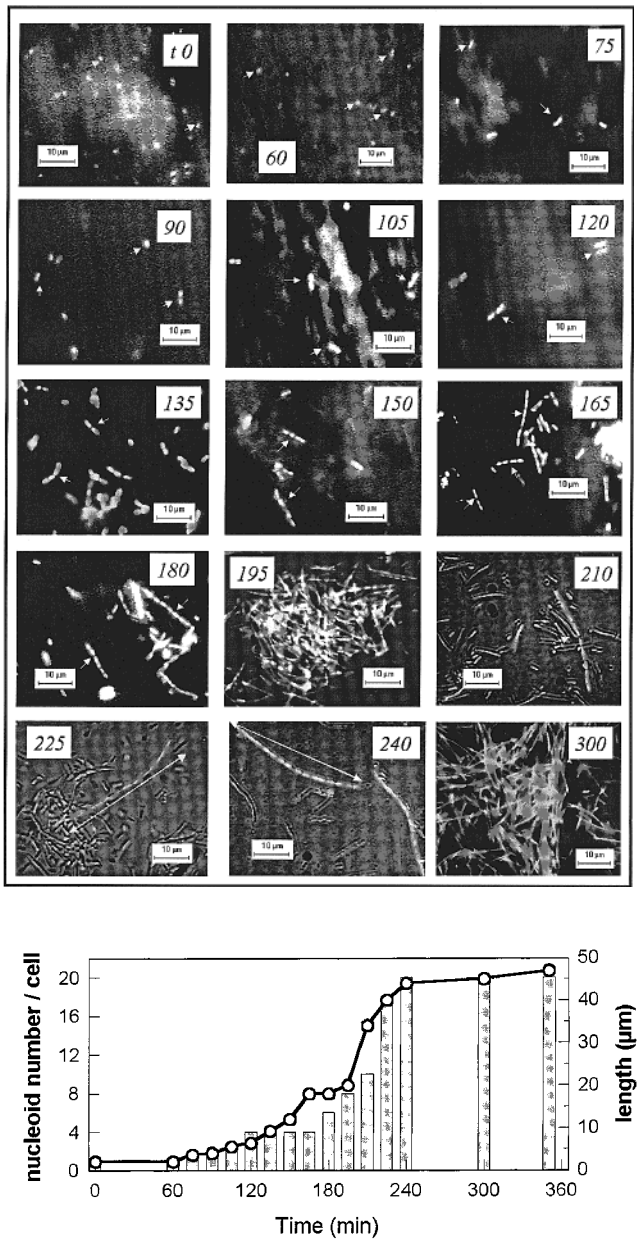

FIGURE 1: *P. mirabilis* elongation occurring during differentiation from vegetative to swarm cells. (Top) Bacteria were visualized after chromosome labeling with DAPI using an epifluorescence microscope. Each panel is labeled after its plating time delay in minutes. Arrows point toward typical bacteria at a particular stage. The long two-headed arrows at 225 and 240 min feature the full length (≈40 μm) of a single elongated bacteria. (Bottom) The differentiation process was quantitatively monitored by measuring the average number of nucleoids per cell (left axis, histogram) and the maximal bacterial length observed (right axis, open circles) at the various times.

the maximal number of nucleoids per cell (about 20) was reached by this time. When determining the number of nucleoids per cell of a number of bacteria from a plate, we observed that the bacteria were homogeneously elongated at any time after seeding, as previously reported in other studies (*20*, *24*). Preliminary IR experiments performed on living bacteria and on purified subcellular extracts (membranes, DNA, or cytosol) assessed that ATR−FTIR spectra of living cells mainly reflect the membranes and their associated components (data not shown). Besides the obvious increases in absorbencies related to the growing biomass with

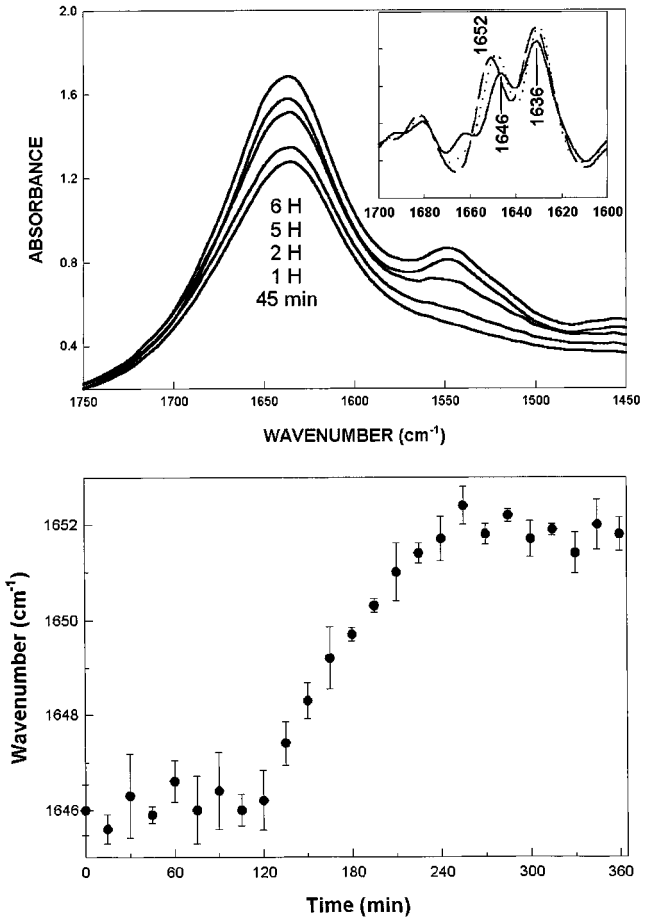

FIGURE 2: Amide I band frequency shift during differentiation. FTIR−ATR spectra were collected every 15 min for 6 h after plating. The upper panels displays (from bottom to top) some of the spectra in the 0.75−6 h time range. The increase in absorbencies (spectra are not offset) is due to the increasing protein content. Second derivative spectra were used to pinpoint the band maxima with a break point of 0.2. The inset of the upper panel displays the inverted second derivatives at 1 h (solid line), 3 h (dotted line), and 5 h (dashed line). The 1636 cm^{-1} peak mainly reflects the water contribution whereas the shifting band (1646 to 1652 cm^{-1}) reflects the protein amide I band. The lower panel displays the evolution with time of the latter derivative peak. Error bars are standard deviations calculated from three independent experiments.

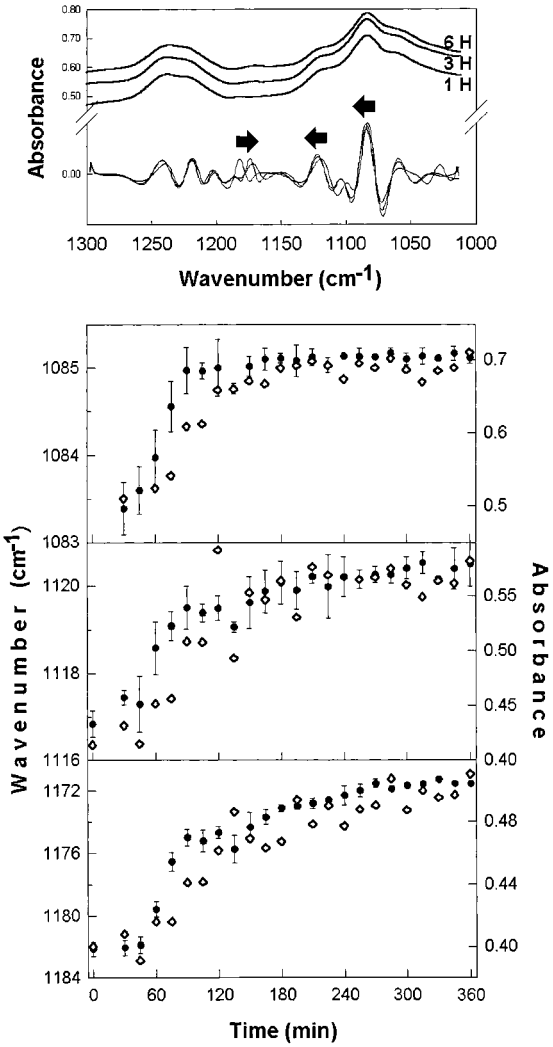

FIGURE 3: Polysaccharide frequency shifts and biosynthesis. The top panel displays three characteristic ATR spectra (upper traces) in the 1300−1000 cm^{-1} frequency domain along with the corresponding inverted second derivatives (lower traces). Arrows feature upshifts or downshifts with time. The three other panels display the evolution of absorbencies and frequencies as a function of time of three vibrational bands reflecting the synthesis of polysaccharides (EPS and LPS) during the *P. mirabilis* differentiation. Experimental conditions and data treatment are similar to those described in Figure 2 (closed circles, wavenumbers; open diamonds, absorbencies).

time, IR spectra were analyzed in terms of frequency shifts during the differentiation from vegetative to swarm cells, which allows to monitor de novo synthesis onsets.

(A) Protein Amide I Band. Figure 2 displays the spectral evolution in the 1750−1450 cm^{-1} frequency domain as a function of time. This domain mainly reflects the water bending mode (1636 cm^{-1}) and the amide I (≈1650 cm^{-1}) and amide II (≈1550 cm^{-1}) bands. When focusing on the $\nu_{C=O}$ frequency domain (1700−1600 cm^{-1}), we observed that the average frequency upshifts with time, as seen from the inset of Figure 2 displaying the second derivative spectra at 1, 3, and 5 h. Clearly, for undifferentiated vegetative cells, the amide I band shows up at 1646 cm^{-1} and progressively upshifts to 1652 cm^{-1} at the end of the differentiation process (Figure 2, lower panel). This upshift is initiated after 2 h and reflects a significant alteration in the average protein population. A $\nu_{C=O}$ frequency of 1652 cm^{-1} indicates that helical secondary structures dominate. As differentiating bacteria become hyperflagellated, we hypothesized that this upshift is mainly due to the massive flagellin assembly into flagellar filaments (*37*). Even though the flagellin secondary structure is only partly (≈40%) α-helical (*38*), our hypothesis is supported by the IR spectra of purified filaments which amide I′ band is located at 1653 cm^{-1}(data not shown), a value very close to that observed in swarm cells. Furthermore, the frequency upshift is concomitant with the onset of *fliC* mRNA accumulation (*24*) (*fliC* encodes flagellin).

(B) Polysaccharides. Drastic alterations of the IR spectra were observed during the differentiation process in the 1000−1200 cm^{-1} frequency domain. We observed frequency shifts for three bands, located at about 1084, 1120, and 1170 cm^{-1}, assigned to carbohydrate backbones present in polysaccharides (Figure 3). Gram-negative bacteria possess an outer membrane, in addition to the cytoplasmic one. The external leaflet of the asymmetric outer membrane is generally composed of only one type of amphipatic molecules, the lipopolysaccharides (LPS) (*39*, *40*). Exopolysaccharides (EPS, also designated CPS for capsular polysaccharides) are

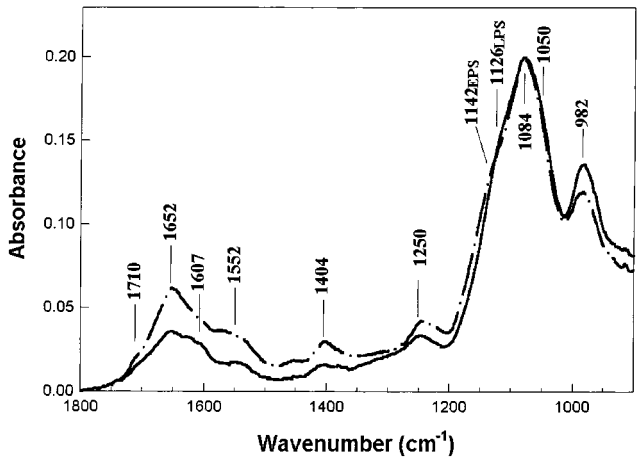

FIGURE 4: ATR−FTIR spectra of dehydrated LPS and EPS extracted from differentiated WT19 *P. mirabilis* cells and slime, respectively. Ten major peaks have been identified from second derivative spectra. Spectra have been normalized for their intensity at 1084 cm^{-1}. LPS, solid line; EPS, dashed−dotted line.

major components of the slime and present a high chemical similarity to the polysaccharide part of LPS. In an attempt to distinguish if the shifting bands observed in living cells arise from either LPS or EPS, we purified the LPS and EPS from *P. mirabilis* cells and slime and determined their IR spectra. As seen in Figure 4, the major IR bands of both dehydrated LPS and EPS spectra are located at 1652 cm^{-1} [ν(C═O) amide I], 1552 cm^{-1} (N−H amide II), 1120−1140 cm^{-1} [ν_{as}(C−O−C) glycosidic linkage], and 1084 and 982 cm^{-1} (complex sugar ring modes). Minor bands are also present at 1710 cm^{-1} [ν(C═O) from *O*-acetyl ester bonds], 1404 cm^{-1} [$\nu_s(COO^-)$], 1250 cm^{-1} [$\nu_s(PO_2^-)$], and 1050 cm^{-1} (carbohydrate backbone). The comparison of EPS and LPS ATR spectra shows that it is the relative contribution, rather than the nature of their constituents, which varies. The major spectral difference between the two fractions is a large shift of the 1126 cm^{-1} component present in LPS up to 1142 cm^{-1} in EPS. This suggests that LPS and EPS must exhibit different branching patterns in their osidic part. However, the strong similarity between LPS and EPS IR spectra does not allow to distinguish the two classes of polysaccharides in whole-cell spectra, since the shifting bands observed in living differentiating cells arise from carbohydrate moieties present in both classes of molecules. Nevertheless, the frequency shifts of the 1084, 1120, and 1170 cm^{-1} bands reflect a qualitative modification in the polysaccharide content during differentiation from vegetative to swarm cells. Clearly, the evolution of these bands is synchronous with biomass production, as shown by the concomitant increase in absorbencies and cell elongation (Figures 1 and 3).

(C) Methylene Stretching Vibrations. The advantage of FTIR spectroscopy for studies of membrane conformational order (*41*−*43*) is that this technique does not require the addition of probe molecules, whose uncertain location in the membrane complicates the extrapolation from the measured spectroscopic properties of the probe to the drawing of accurate conclusions about changes in membrane properties (*43*). This is particularly critical for Gram-negative bacteria, since the distribution of an extrinsic probe between the outer and the cytoplasmic membranes is difficult to resolve. The symmetric CH_2 stretching band $\nu_s(CH_2)$ near 2850 cm^{-1} is

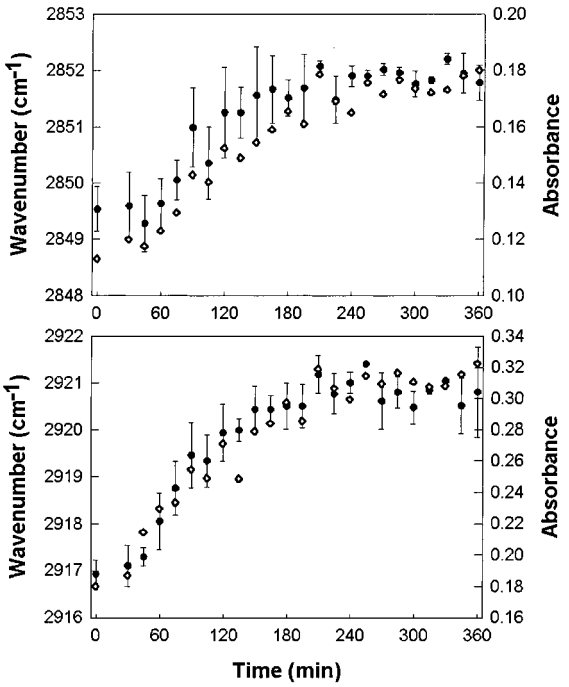

FIGURE 5: Frequencies of the $\nu_s(CH_2)$ and $\nu_{as}(CH_2)$ vibrations as a function of time. Experimental conditions and data treatment are similar to those described in Figure 2. Symbols are as in Figure 3.

particularly valuable for probing the "state of order" of biological membranes, since its frequency sensitively responds to order/disorder transitions and to changes in the mobility of the fatty acid chains. The methylene stretching vibrations near 2920 and 2850 cm^{-1} have been hence frequently used to probe the fluidity of biological membranes, since the frequencies of these bands shift to higher wavenumbers upon introduction of gauche rotamers (promoting disorder) into the acyl chains (*44*). Inspection of the IR spectra of bacteria undergoing the differentiation process in the 2000−3000 cm^{-1} frequency domain revealed that the ν_s (2850 cm^{-1}) and ν_{as} (2920 cm^{-1}) methylene vibrations of fatty acids undergo significant upshifts of 2.5 and 4 cm^{-1}, respectively (Figure 5), showing a more disordered state in differentiated bacteria. These upshifts are correlated in time to the increase in absorbance, linking de novo synthesis of fatty acids to increased membrane disorder. Moreover, the time evolution of these frequencies matches those of polysaccharides described above.

Thermotropic Response of Isolated Membranes. The above results prompted us to investigate the thermal response of isolated membranes of both cell types to measure the temperature of the gel/liquid crystal phase transition. As usually observed for other Gram-negative bacteria (*45*), the IR spectra of purified membranes at temperature below 20 °C are characteristic of membranes in the gel phase, whereas the IR spectra above 40−50 °C are characteristic of membranes in the conformationally disordered liquid crystal phase. This is also true for *P. mirabilis*, since, regardless the differentiation state, similar low $\nu_s(CH_2)$ frequencies observed below 25 °C upshift at higher temperatures (Figure 6). In fact, it is the transition temperature (T_m) which is significantly altered during differentiation, since it decreased from 42.3 ± 0.7 °C (vegetative cells) to 33.0 ± 0.7 °C (swarm cells). It implies that, at the growth temperature (37 °C), vegetative cells are below their membrane T_m, whereas

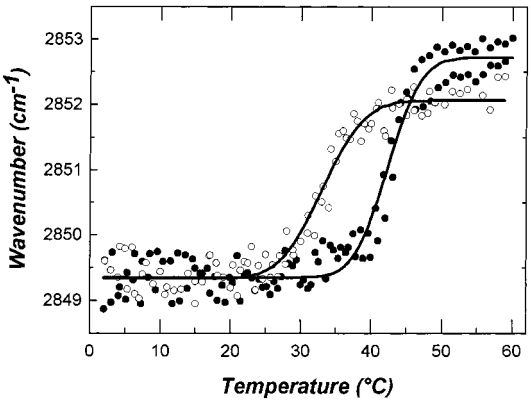

FIGURE 6: Temperature dependence of the $\nu_s(CH_2)$ symmetric stretching frequency of membranes extracted from vegetative (●) and swarm (○) *P. mirabilis* WT19 cells. IR spectra were collected, and raw data were fitted by using a cumulative normal distribution law (solid line) to yield T_m values of 42.3 ± 0.7 °C (vegetative cells) and 33.0 ± 0.7 °C (swarm cells). Cooperativity estimated from the width of the normal distribution model is 3.7 and 4.7 for vegetative and swarm cells, respectively. Data are from three independent experiments.

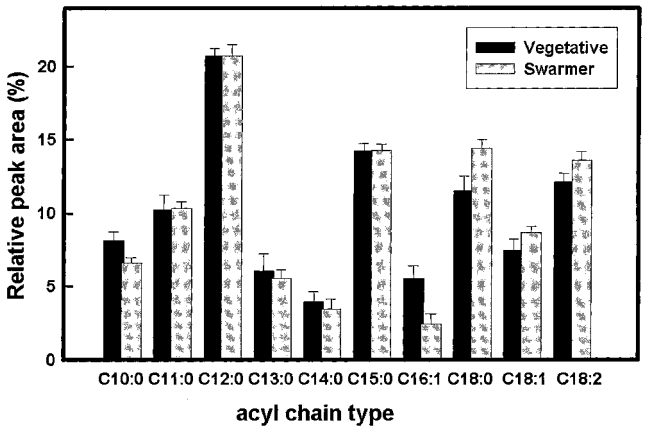

FIGURE 7: Gas chromatographic analysis of membrane fatty acid composition from P19 vegetative and swarm cells. The total area of the detectable GC peaks of the chromatogram obtained from each membrane preparation was set to 100%. The individual GC peaks were then calculated in relative percent of the total area. Typical errors in the peak areas are within 5%, which yield an estimated uncertainty in the fatty acid relative content of ~0.6% (error bars for three experiments).

swarm cells are above this transition. We conclude that differentiated cells exhibit significantly increased membrane fluidity. This likely results from a modification of the lipid composition of bacterial membranes. Besides, it is interesting to note that, for both cell types, the $\nu_s(CH_2)$ wavenumbers of purified membrane fractions observed at 37 °C exactly match those observed in living bacteria. Thus the decrease in the T_m values observed in isolated membranes confirms the distinct frequencies observed in living bacteria.

We determined the fatty acid relative composition of lipids from membranes of vegetative and swarm cells by gas chromatography. Figure 7 displays the relative areas, in percentage of the total area, of the peaks detected and assigned in the GC traces from membrane preparations of wild-type bacteria. In a first approximation, the amounts of C10:0 to C15:0 chains [mainly present in LPS of the outer membrane (*46*)] are constant. It is the palmitoleic (C16:1) chain whose proportion is reduced by a 2.3 factor in swarm cells at the benefit of longer C18 chains of various degrees of unsaturation: C18:0, C18:1, and C18:2. This increased content in longer fatty acid chains fits well with the T_m reduction observed in swarm cells since longer and less saturated acyls chains will favor the occurrence of gauche conformers and hence increase the disorder (which increases from the periphery to the center of the bilayer) as the temperature rises and will thereby promote the gel-to-liquid transition. This demonstrates that *P. mirabilis* differentiation includes a variation in membrane lipid composition, which likely constitutes a major cause of the increased membrane fluidity observed in swarm cells.

DISCUSSION

P. mirabilis swarming features one of the most striking manifestations of bacterial multicellular behavior by its robust synchronicity (*5*−*8*), its ability to adapt to a brand new environment and to cooperate. This necessarily implies that the cell machinery turns to new biosyntheses in order to cope with the physicochemical characteristics of the solid substratum to colonize. The present study is the first to focus on the biochemical alterations linked to the differentiation process of *P. mirabilis*. It appears that extracellular material and membranes are substantially modified during the bacterial morphogenesis. We observed the massive appearance of surface or extracellular proteins exhibiting significant helical content. This very likely reflects the assembly of flagellin into extracellular flagellar filaments, consistently with our IR spectra of extracted filaments, and the hyperflagellation of differentiated *P. mirabilis* (*6*). This is not new information, but it confirms that our approach yields biologically significant results. This study also provides evidence for thus far unreported modifications occurring concomitantly with cell elongation. We observed frequency shifts in bands reflecting LPS and EPS, showing qualitative modifications associated with these molecules. These modifications must originate in the distinct IR spectra of the two classes of polysaccharide molecules which are de novo synthesized during the elongation process. The importance of an EPS (designated Cmf) for *P. mirabilis* mass migration and uropathogenicity was previously reported (*11*, *17*). It was recently shown that LPS play a critical role for the swarming of *Salmonella enterica* serovar Typhimurium (*9*). The authors propose that LPS can be converted to EPS during swarming, contributing to the external slime. This does not seem to occur in *P. mirabilis* since LPS and EPS exhibit different glycosidic linkages. Toguchi et al. (*9*) furthermore hypothesized not only that the slime is essential to colony expansion but also that its polysaccharides constitute a differentiation-inducing signal explaining the cell density dependence of swarming in a model which would also apply to *P. mirabilis*. Increased production of slime (and therefore of its polysaccharides) was logically expected during differentiation and swarming, but the qualitative alterations shown by our results were less obviously predicted. We also observed that the membrane fluidity is increased in swarm cells, as compared to vegetative ones. This is explained by changes in the ratio between fatty acid chains of membrane lipids. This fluidity increase could correspond to an adaptation of the bacteria to their physical environment (solid surface conditioned with slime) or could also have a regulatory function, either by directly changing the activity of membrane proteins (*47*) or

by influencing lateral diffusion (and therefore subcellular location) within the membranes (*48*).

In situ monitoring of living bacteria by FTIR−ATR spectroscopy allowed the definition of the time course of relevant biosyntheses. Syntheses of LPS and EPS qualitatively distinct from those of vegetative cells are synchronous with the alteration of membrane fatty acid chains. Frequency shifts of the corresponding bands appeared clearly around 60 min after plating, when we could observe the beginning of the elongation process. The frequency shift of protein amide I band, which mainly reveals the assembly of flagellin in extracellular filaments, became only apparent after an additional delay of about 60 min. Karlinsey et al. (*49*) observed a delay of 45 min between the transcription of *flhDC* and the appearance of nascent flagellar filaments at the surface of *Salmonella typhimurium* cells. A delay of this range in *P. mirabilis* would indicate that cell elongation and flagella biogenesis, two FlhDC-dependent processes (*24*, *30*), are initiated at about the same time but become observable after different incubation periods. All frequency shifts are completed about 180 min after plating, except the protein amide I band, which upshifts until 240 min of incubation, when maximal cell elongation is reached.

The present data show that some of the biochemical events involved in the differentiation process do not occur in a synchronous manner but rather sequentially, since membrane maturation and LPS−EPS synthesis occur prior to hyperflagellation. These time courses suggest that the macroscopic timing (periodicity) of *P. mirabilis* swarming may rely on a complex array of events, each one embedded in time through its correlation with the preceding and following steps as suggested by the kinetic model proposed by Esipov and Shapiro (*50*), rather than on a singular chemical trigger. As mentioned in the introduction, such a complex behavior necessarily implies a high degree of signal integration. To address these points, it is now necessary to resolve in time and space the *P. mirabilis* dimorphism within a swarming colony. The present study reveals that vegetative and swarm cells exhibit distinct IR spectral signatures. A state of the art IR microscope allows monitoring 50 μm spots on nearly every surface and, hence, fulfills the requirements for an investigation of the space and time distribution of each cell type within *P. mirabilis* colonies. Preliminary experiments performed in our laboratory with a Continuμm (Nicolet) IR microscope equipped with a Ge ATR crystal confirmed the feasibility of spectrally resolving the different spatial domains (inoculum, consolidation, periphery) of the *P. mirabilis* colony growing on a Petri dish agar surface. This next step must provide us with a better understanding of the *P. mirabilis* dynamics by achieving in situ noninvasive metabolic imaging of the colony. Widening the framework of this study, it can be safely assessed that multicellularity could be monitored on various living systems without strongly interfering with the system investigated. By providing space and time-resolved metabolic snapshots of complex biological systems, infrared microscopy will certainly contribute to our understanding of integration and multiple feedback processes.

ACKNOWLEDGMENT

The authors are greatly indebted to Marie-Joseph Bertrand and Mikael Berrou for technical assistance in lipid analyses. The *Proteus* strain was a generous gift from Dr. C. Hughes (University of Cambridge, U.K.).

REFERENCES

1. Shapiro, J. A. (1995) *BioEssays 17*, 597−607.
2. Shapiro, J. A. (1998) *Annu. Rev. Microbiol. 52*, 81−104.
3. Harshey, R. M. (1994) *Mol. Microbiol. 13*, 389−394.
4. Eberl, L., Molin, S., and Givskov, M. (1999) *J. Bacteriol. 181*, 1703−1712.
5. Fraser, G. M., and Hughes, C. (1999) *Curr. Opin. Microbiol. 2*, 630−635.
6. Allison, C., and Hughes, C. (1991) *Mol. Microbiol. 5*, 1975−1982.
7. Rauprich, O., Matsushita, M., Weijer, C. J., Siegert, F., Esipov, S. E., and Shapiro, J. A. (1996) *J. Bacteriol. 178*, 6525−6538.
8. Matsuyama, T., Takagi, Y., Nakagawa, Y., Itoh, H., Wakita, J., and Matsushita, M. (2000) *J. Bacteriol. 182*, 385−393.
9. Toguchi, A., Siano, M., Burkart, M., and Harshey, R. M. (2000) *J. Bacteriol. 182*, 6308−6321.
10. Rahman, M. M., Guard-Petter, J., Asokan, K., Hughes, C., and Carlson, R. W. (1999) *J. Biol. Chem. 274*, 22993−22998.
11. Gygi, D., Rahman, M. M., Lai, H. C., Carlson, R., Guard-Petter, J., and Hughes, C. (1995) *Mol. Microbiol. 17*, 1167−1175.
12. Belas, R., Erskine, D., and Flaherty, D. (1991) *J. Bacteriol. 173*, 6279−6288.
13. Belas, R., Goldman, M., and Ashliman, K. (1995) *J. Bacteriol. 177*, 823−828.
14. Allison, C., Lai, H.-C., and Hughes, C. (1992) *Mol. Microbiol. 6*, 1583−1591.
15. Allison, C., Coleman, N., Jones, P. L., and Hughes, C. (1992) *Infect. Immun. 60*, 4740−4746.
16. Rózalski, A., Sidorczyk, Z., and Kotelko, K. (1997) *Microbiol. Mol. Biol. Rev. 61*, 65−89.
17. Allison, C., Emödy, L., Coleman, N., and Hughes, C. (1994) *J. Infect. Dis. 169*, 1155−1158.
18. Stickler, D., Morris, N., Moreno, M.-C., and Sabbuba, N. (1998) *Eur. J. Clin. Infect. Dis. 17*, 649−652.
19. Allison, C., Lai, H.-C., Gygi, D., and Hughes, C. (1993) *Mol. Microbiol. 8*, 53−60.
20. Gygi, D., Bailey, M. J., Allison, C., and Hughes, C. (1995) *Mol. Microbiol. 15*, 761−769.
21. Gygi, D., Fraser, G., Dufour, A., and Hughes, C. (1997) *Mol. Microbiol. 25*, 597−604.
22. Belas, R., Schneider, R., and Melch, M. (1998) *J. Bacteriol. 180*, 6126−6139.
23. Eberl, L., Christiansen, G., Molin, S., and Givskov, M. (1996) *J. Bacteriol. 178*, 554−559.
24. Furness, R. B., Fraser, G. M., Hay, N. A., and Hughes, C. (1997) *J. Bacteriol. 179*, 5585−5588.
25. Hay, N. A., Tipper, D. J., Gygi, D., and Hughes, C. (1997) *J. Bacteriol. 179*, 4741−4746.
26. Dufour, A., Furness, R. B., and Hughes, C. (1998) *Mol. Microbiol. 29*, 741−751.
27. Claret, L., and Hughes, C. (2000) *J. Bacteriol. 182*, 833−836.
28. Prüss, B. M., and Matsumura, P. (1996) *J. Bacteriol. 178*, 668−674.
29. Claret, L., and Hughes, C. (2000) *J. Mol. Biol. 303*, 467−478.
30. Chilcott, G. S., and Hughes, K. T. (2000) *Microbiol. Mol. Biol. Rev. 64*, 694−708.
31. Porter, K. G., and Feig, Y. S. (1980) *Limnol. Oceanogr. 25*, 943−948.
32. Siegers, K., Heinzmann, S., and Entian, K.-D. (1996) *J. Biol. Chem. 271*, 12294−12301.
33. Inzana, T. J. (1983) *J. Infect. Dis. 148*, 492−499.
34. Folch, J., Lees, M., and Sloane-Stanley, G. H. (1957) *J. Biol. Chem. 226*, 497−509.
35. Cameron, D. G., and Moffatt, D. J. (1987) *Appl. Spectrosc. 41*, 539−544.

36. Dong, H., Huang, P., and Caughey, W. S. (1990) *Biochemistry 29*, 3303−3308.
37. Aizawa, S.-I. (1996) *Mol. Microbiol. 19*, 1−5.
38. Samatey, F. A., Imada, K., Nagashima, S., Vonderviszt, F., Kumasaka, T., Yamamoto, M., and Namba, K. (2001) *Nature 410*, 331−337.
39. Brass, J. M. (1986) *Curr. Top. Microbiol. Immunol. 129*, 1−92.
40. Huijbregts, R. P. H., de Kroon, A. I. P. M., and de Kruijff, B. (2000) *Biochim. Biophys. Acta 1469*, 43−61.
41. Cameron, D. G., Martin, A., Moffatt, D. J., and Mantsch, H. H. (1985) *Biochemistry 24*, 4355−4359.
42. Moore, D. J., Wyrwa, M., Reboulleau, C. P., and Mendelsohn, R. (1993) *Biochemistry 32*, 6281−6287.
43. Moore, D. J., and Mendelsohn, R. (1994) *Biochemistry 33*, 4080−4085.
44. Snyder, R. G. (1967) *J. Chem. Phys. 47*, 1316−1360.
45. Naumann, D., Schultz, C. P. and Helm, D. (1996) in *Infrared Spectroscopy of Biomolecules* (Mantsch, H. H., and Chapman, D. Eds.) pp 279−310, Wiley-Liss, New York.
46. Schultz, C., and Naumann, D. (1991) *FEBS Lett. 294*, 43−46.
47. Hazel, J. R., and Williams, E. E. (1990) *Prog. Lipid Res. 29*, 167−227.
48. Losick, R., and Shapiro, L. (1999) *J. Bacteriol. 181*, 4143−4145.
49. Karlinsey, J. E., Tanaka, S., Bettenworth, V., Yamaguchi, S., Boos, W., Aizawa, S.-I., and Hughes, K. T. (2000) *Mol. Microbiol. 37*, 1220−1231.
50. Esipov, S. E., and Shapiro, J. A. (1998) *J. Math. Biol. 36*, 249−268.

BI010434M